

Level repulsion in hybrid photonic-plasmonic microresonators for enhanced biodetection

Matthew R. Foreman* and Frank Vollmer

Max Planck Institute for the Science of Light, Laboratory of Nanophotonics and Biosensing,
Günther-Scharowsky-Straße 1, 91058 Erlangen, Germany

We theoretically analyse photonic-plasmonic coupling between a high Q whispering gallery mode (WGM) resonator and a core-shell nanoparticle. Blue and red shifts of WGM resonances are shown to arise from crossing of the photonic and plasmonic modes. Level repulsion in the hybrid system is further seen to enable sensitivity enhancements in WGM sensors: maximal when the two resonators are detuned by half the plasmon linewidth. Approximate bounds are given to quantify possible enhancements. Criteria for reactive vs. resistive coupling are also established.

DOI: [10.1103/PhysRevA.88.023831](https://doi.org/10.1103/PhysRevA.88.023831)

PACS number(s): 42.79.Gn, 73.20.Mf, 78.67.Bf, 87.80.Nj

I. INTRODUCTION

Optical microresonators play an important role in modern day physics, for example, enabling study of cavity quantum electrodynamic phenomena, tailoring of spontaneous emission spectra of atoms and quantum dots, spectral filtering and development of novel light sources [1]. Combination of optical microresonators with metallic nanoparticles (NPs) supporting localised surface plasmons (LSPs) has also recently attracted much attention, due to the opportunities it affords in efficient light routing, field confinement and enhanced spectroscopy [2–5]. One further field of importance is that of whispering gallery mode (WGM) biosensing where large reactive coupling to dielectric particles, such as bacteria and proteins, results in detectable WGM frequency shifts [6, 7]. In the drive for single molecule sensitivity, enhancement of reactive shifts and maximisation of near field intensities are, however, necessary [8] such that plasmonic NPs are being increasingly employed as either analyte labels [9–11] or near field nanoantennae [5, 12, 13]. Sensitivity enhancements specifically derive from the increased polarisability of NPs and generation of plasmonic hotspots, which are maximum when operating at wavelengths close to the LSP resonance of the NP. Near resonance, however, scattering and absorption losses are also increased such that resonance quality is degraded hence counteracting potential sensitivity gains. A balance must hence be struck. In this article we therefore consider the hitherto overlooked phenomena of level repulsion and level crossings in NP coupled high Q microresonators, arising from reactive and resistive coupling contributions, which in turn allows optimal NP configurations to be identified. Whilst we consider the case of core-shell NPs coupled to spherical whispering gallery mode resonators (WGMRs) for simplicity, the underlying physical principles are common to all resonator geometries and are hence applicable in a broader sense.

The structure of this article is as follows. In Section II we derive and discuss the hybridisation of photonic and LSP resonant modes, whereby we demonstrate both level repulsion and crossing. We proceed in Section III to con-

sider the consequences of this mode hybridisation within the context of WGM biosensing, in turn allowing the optimal NP geometry to be found, as is dictated by the detuning of the WGM and LSP resonances. Concluding remarks are made in Section IV.

II. MODE HYBRIDISATION IN COUPLED PHOTONIC-PLASMONIC SYSTEMS

Resonances in isolated microcavities have been well studied in the literature [14–16] and in all cases can be cast into a secular equation: $|\mathbb{G}| = 0$, where \mathbb{G} is an appropriate system matrix. Energy can, in general, escape from the resonator (e.g. via radiation and absorption losses), such that \mathbb{G} is non-Hermitian and the associated eigenvalues (and hence resonance frequencies) are complex. For example, for spherical microresonators \mathbb{G} is a diagonal matrix with non-zero elements given by $1/\eta_l^\nu$ [17], where η_l^ν are the well known Mie scattering coefficients for transverse electric (TE, $\nu = M$) or magnetic (TM, $\nu = E$) Mie modes with polar and azimuthal mode indices (l, m) [14]. Accordingly the secular equation decouples in l and m to yield the more familiar transcendental equation (which is independent of m):

$$\frac{[n_I z h_l(n_I z)]'}{h_l(n_I z)} = N \frac{[n_{II} z j_l(n_{II} z)]'}{j_l(n_{II} z)}, \quad (1)$$

where $N = 1$ or $(n_I/n_{II})^2$ for TE or TM modes respectively, $j_l(x)$ and $h_l(x)$ are the spherical Bessel and Hankel functions of the first kind, $z = ka$, k is the (complex) vacuum wavenumber, a is the resonator radius, prime denotes differentiation with respect to the argument of the respective Hankel or Bessel function and n_I (n_{II}) is the refractive index of the surrounding medium (resonator). It should be noted that Eq. (1) is conventionally found by directly considering when the denominator of η_l^ν is zero. Whilst many solutions to Eq. (1) can be found, here we will primarily be interested in bound surface modes, i.e. WGMRs, for which $\text{Re}[z] \sim l/n_{II}$ [18].

Plasmonic resonances in metallic NPs have similarly seen extensive research in the literature. Small ($\ll \lambda$) homogeneous NPs, for instance, are often described using a (complex) polarisability given by the Clausius-Mossotti relation, such that LSP resonance occurs when the Fröhlich condition is satisfied [19] (as again follows by

*matthew.foreman@mpl.mpg.de

considering when the denominator of the polarisability is zero). This treatment is, however, only approximate and breaks down for larger, or inhomogenous, NPs due to retardation effects and field non-uniformity. More generally, the exact polarisability, α_{Mie} , of a (possibly inhomogenous) spherical NP can be found using generalised Mie theory, or the T -matrix method [20, 21] viz.

$$\alpha_{\text{Mie}} = -4\pi \frac{3i}{2k^3 \epsilon_1^{3/2}} T_1^E \quad (2)$$

where T_1^E is the electric dipole element of the T -matrix and $\epsilon_1 = n_1^2$ is the electric permittivity of the medium surrounding the NP [22]. For homogeneous NPs $T_1^E = \eta_1^E$, whilst for core-shell NPs $T_1^E = \kappa_1^E$ (as defined in Appendix C of [17]). Evidently, the methodology adopted to determine LSP resonances in metallic NPs is formally, and physically, equivalent to that used for determining resonances in large microcavities. When considering more general resonator and NP geometries, similar arguments can also be made, albeit the form of \mathbb{G} becomes more complicated and separability in l and m (or analogous mode indices) is likely lost.

When a NP is coupled to a microcavity the mode structure of the combined system is modified, yielding hybrid photonic-plasmonic modes with resonance frequencies shifted from the bare resonator case. Hybrid resonances, can again be found by solution of the equation $|\mathbb{G}| = 0$, albeit coupling terms must be incorporated into \mathbb{G} . In earlier work, we have derived the appropriate system matrix describing coupling of arbitrary NPs to spherical WGMRs [17], whereupon resonance conditions were found for hybridisation of the electric dipole LSP resonance in a NP with the TE and TM WGMRs. Restricting attention, henceforth, to a core-shell NP the resonance conditions are (approximately) given by [17]:

$$0 = \frac{1}{\eta_l^\nu \kappa_1^E} - \tilde{\mathcal{U}}_{lm}^{lm} \mathcal{U}_{lm}^{1m}, \quad (3)$$

where $\mathcal{U}_{lm}^{1m} = \mathcal{A}_{lm}^{1m}$ or \mathcal{B}_{lm}^{1m} are the translation coefficients for TM and TE modes respectively, which arise when relating fields from displaced scatterers. In the absence of coupling, Eq. (3) reduces to the resonance conditions for the isolated WGMR ($1/\eta_l^\nu(k) = 0$) and NP ($1/\kappa_1^E(k) = 0$) as discussed above, whilst the coupling (embodied in $\tilde{\mathcal{U}}_{lm}^{lm} \mathcal{U}_{lm}^{1m}$) represents a perturbation to these conditions. It must be emphasised that symmetry dictates that the quantisation (polar) axis is defined along the line joining the WGMR and NP centers, hence avoiding coupling between azimuthal modes.

Realistically, the broad LSP resonance spectrally overlaps with multiple polar modes (of both high and low Q) within the WGMR, a point neglected in the derivation of Eq. (3). Upon inclusion of this effect, the resonance conditions can be written in the form:

$$0 = 1 - \kappa_1^\nu \sum_{l=0}^{\infty} \eta_l^E \tilde{\mathcal{U}}_{lm}^{lm} \mathcal{U}_{lm}^{1m}. \quad (4)$$

The real and imaginary parts of the complex roots of Eqs. (3) and (4) define the resonance frequency and linewidth of the hybrid modes (here termed ‘‘quasi-TM’’

and ‘‘quasi-TE’’) respectively. Noting that $\mathcal{A}_{lm}^{1m} = 0$ for $|m| > 1$ and $\mathcal{B}_{lm}^{1m} = 0$ for $|m| \neq 1$, it is evident that only the low order azimuthal modes hybridise, whilst higher order azimuthal modes remain unperturbed. Physically this is a consequence of higher order modes having zero intensity at the site of the NP.

Greater insight into Eq. (4) can be gained by considering the case when the LSP peak lies spectrally close to the WGMR resonance of polar index L , as can be practically realised using the tunability of core-shell NPs [23]. Near resonance the scattering coefficients can be represented by complex Lorentzians of the form

$$\chi_l^{\nu,j}(k) \approx \chi_l^{\nu,j}(k_{0,j}) \frac{i\Gamma_{0,j}/2}{(k - k_{0,j}) + i\Gamma_{0,j}/2}, \quad (5)$$

where $\chi_l^{\nu,j} = \eta_l^\nu$ or κ_l^ν for $j = 1$ and 2 respectively and $k_j = k_{0,j} - i\Gamma_{0,j}/2$ ($k_{0,j}, \Gamma_{0,j} \in \mathbb{R}$) is the complex resonance frequency of an isolated WGMR ($j = 1$) and NP ($j = 2$). Note that both the resonance frequency $k_{0,j}$ and linewidth $\Gamma_{0,j}$ depend on the mode indices (ν, l, m), however this dependence has been suppressed for clarity. We also note for later convenience that $\chi_l^{\nu,j}(k_{0,j}) \in \mathbb{R}$.

Upon substituting Eq. (5) into Eq. (4) and subsequent rearrangement we arrive at the quadratic equation :

$$k_{12}^2 - k_{12}(k_1 + k_2 - iJ) + k_1 k_2 = -ik_1 J - K \quad (6)$$

where $k_{12} = k_{0,12} - i\Gamma_{0,12}/2$ is the complex resonance frequency of the hybrid mode,

$$J = \frac{1}{2} \Gamma_{0,2} \kappa_1^E(k_{0,2}) \sum_{l \neq L} \eta_l^\nu(k_{0,1}) \tilde{\mathcal{U}}_{lm}^{lm} \mathcal{U}_{lm}^{1m} \quad (7)$$

describes the strength of coupling between the LSP and off-resonance ($l \neq L$) modes and

$$K = \frac{1}{4} \Gamma_{0,1} \Gamma_{0,2} \eta_L^\nu(k_{0,1}) \kappa_1^E(k_{0,2}) \tilde{\mathcal{U}}_{lm}^{lm} \mathcal{U}_{lm}^{1m} \quad (8)$$

describes coupling between the LSP and the on-resonance ($l = L$) WGMR. Completing the square in Eq. (6) yields

$$\delta k_j = \frac{1}{2} \left[(k_1 + k_2 - 2k_j - iJ) \pm \sqrt{(k_1 + k_2 - iJ)^2 - 4(k_1 k_2 + ik_1 J + K)} \right], \quad (9)$$

where $\delta k_j = k_{12} - k_j$. Eq. (9) describes hybridisation of the LSP and WGMR resonances giving rise to a level crossing. Figure 1 shows the extinguished power (here letting $J = 0$ for illustrative purposes) of a WGMR-NP system, illuminated by a field which would excite a TM (40, 1) WGMR in an isolated WGMR, as a function of the WGMR-LSP resonance detuning (as can be parameterised by the ratio $f = r_{II}/r_{IV}$ of the core-shell NP radii - see inset of Figure 2), from which the crossing behaviour is evident. We note that there is an anticrossing in the imaginary part of k_j , i.e. linewidth. For calculation purposes the WGMR was assumed to have a refractive index of $n_{II} = 1.59$, radius of $r_{II} = 4 \mu\text{m}$ and to be in air ($n_I = 1$), such that the (40, 1) TM WGMR resonance is at a wavelength of 772.459 nm (the second order radial

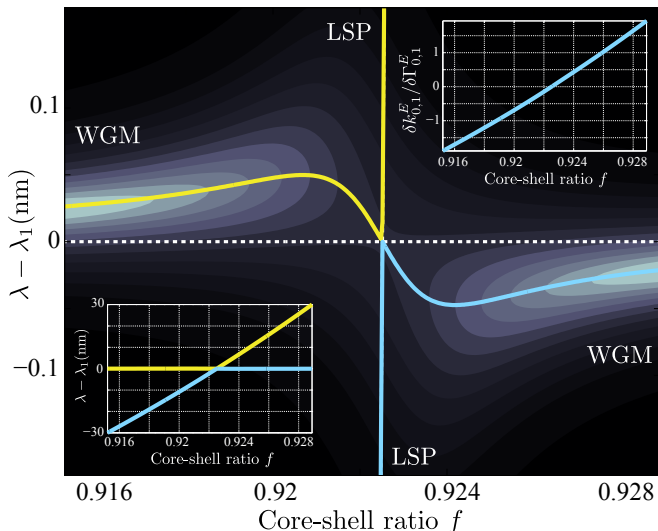


FIG. 1: (Color online) Normalised extinction spectrum vs. ratio of core-shell radii for a coupled WGMR-NP system illuminated to excite the (40, 1) WGM in a bare WGMR. Solid lines show resonance branches defined by Eq. (9). Left inset: larger scale view of resonance branches. Right inset: ratio of resonance shift, $\delta k_{0,1}^E$, to line broadening, $\delta \Gamma_{0,1}^E$, quantifying reactive vs resistive coupling.

WGM was considered as was discussed in [17]). Furthermore, a core-shell NP, of outer radius $r_{III} = 32$ nm, with a fused silica ($n_{IV} = 1.48$) core and silver shell was taken and assumed to be bound at the surface of the WGMR. The permittivity of silver was modelled using a Drude-Lorentz model whereby $\epsilon_{III}(\omega) = \epsilon_\infty - \omega_p^2/(\omega^2 + i\omega\gamma)$. Values of $\epsilon_\infty = 3.7$, $\omega_p = 8.9$ eV and $\gamma = 0.021$ eV were taken. In reality we note that the dielectric function of metallic layers becomes size dependent when the layer thickness is small in relation to the mean-free path of electrons [24]. In turn, this causes a broadening of the LSP resonance due to additional surface collisions of the electrons in the metal, however, use of a more realistic permittivity function, such as that presented in [25], does not affect the physical conclusions of this article, such that a Drude-Lorentz model was adopted for simplicity.

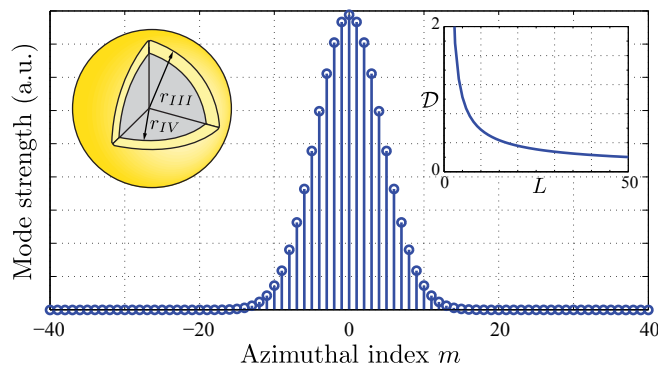


FIG. 2: (Color online) Mode strengths of degenerate azimuthal modes in a fundamental $L = 40$ WGM. Left inset: geometry of a core-shell NP. Right inset: variation of the ratio $D = \sum_{|m| \le 1} |D_m|^2 / \sum_{2 \le |m| \le L} |D_m|^2$ with polar index L .

Solid lines in Figure 1 depict the resonance branches defined by Eq. (9), which swap nature as the resonance detuning changes sign. Due to the small size of the NP, resonance shifts of the WGM-like resonance are of the order of picometers, such that the LSP-like branches appear as near vertical lines in Figure 1 (see left inset for a larger scale view). Strong extinction is not seen on the LSP branches since we assume the LSP is only excited through leakage from the WGMR. From Figure 1 it can be seen that for larger detunings the WGM and LSP modes are mutually repelled, however at small detunings the repulsion effect diminishes, the WGM resonance broadens due to increased scattering and absorption losses arising from stronger (resistive) coupling to the NP, and ultimately the resonance branches cross. An optimal NP core-shell ratio can hence be identified whereby reactive resonance shifts are maximised, as shall be determined analytically in what follows.

III. OPTIMAL RESONANCE SHIFTS IN WGM BIOSENSING

WGM based sensors operate by what has become known as the reactive sensing principle [26]. Specifically, the spectral position of a WGM resonance is shifted when a molecule enters the near field of the WGMR, by an amount proportional to the polarisability of the particle. Typical shifts of WGM resonances in biosensing experiments are, however, on the femtometer scale, such that the shift of the $m = 1$ WGM mode depicted in Figure 1 is comparatively large. However, due to the choice of polar axis, excitation of a fundamental WGM, commonly used for sensing and considered as a single mode, must be represented by a superposition of degenerate azimuthal modes [27]. Since only the low order azimuthal modes are perturbed (hence lifting the degeneracy) the total extinction spectrum is formed by superposition of $2L - s$ unshifted resonances ($s = 2$ or 1 for quasi-TM and -TE modes respectively) with $s + 1$ shifted modes viz.

$$C_{\text{ext}}(k) = C_0 \sum_{l=0}^{\infty} \sum_{m=-l}^l A_m \frac{\Gamma_{0,12}^2}{4(k - k_{0,12})^2 + \Gamma_{0,12}^2}. \quad (10)$$

Here a Lorentzian mode profile has again been adopted and the dependence of each quantity on (ν, l, m) is again suppressed. C_0 is an appropriate normalisation constant and A_m denotes the strength of each azimuthal mode and is dependent on the illuminating field [17]. Summation over l in Eq. (10) accounts for additional non-resonant contributions to the total extinction spectrum from $l \neq L$ polar modes. In practise the summation limits can be truncated since realistic coupling schemes for WGMRs excite a limited range of polar modes [28].

To determine the apparent shift of the measured WGM resonance lineshape (as dictated by the superposition of both shifted and unshifted azimuthal modes) the spectral position, k_{max} of the maximum in Eq. (10) must be found. Therefore, we differentiate Eq. (10) with respect to k and equate the result to zero as per standard theory,

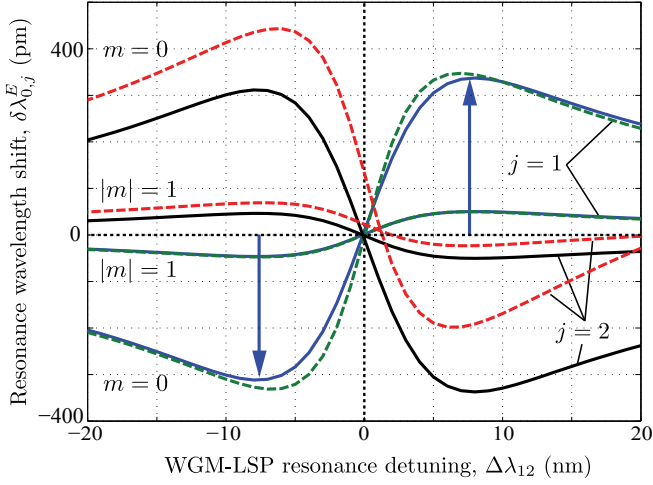


FIG. 3: (Color online) Resonance shifts of $|m| \leq 1$ quasi-TM modes for $j = 1$ (blue and green) and $j = 2$ (black and red). Solid (dashed) curves denote shifts calculated using Eq. (13) (Eq. (3)). Arrows denote detunings of $\pm\Gamma_{0,2}/2$ (see Eq. (21)).

ultimately yielding

$$0 = \sum_{|m| \leq 1} A_m \frac{\Gamma_{0,12}^2 (k_{\max} - k_{0,1} - \delta k_{0,1})}{[4(k_{\max} - k_{0,1} - \delta k_{0,1})^2 + \Gamma_{0,12}^2]^2} + \sum_{2 \leq |m| \leq L} A_m \frac{\Gamma_{0,1}^2 (k_{\max} - k_{0,1})}{[4(k_{\max} - k_{0,1})^2 + \Gamma_{0,1}^2]^2} \quad (11)$$

where $\delta k_{0,j} = \text{Re}[\delta k_j]$ and the non-resonant contributions are assumed to vary negligibly with wavenumber near the WGM resonance. Broadening of a single $|m| \leq 1$ mode is well described by Larmor's formula for an oscillating dipole [29], however, for our purposes it is safe to neglect broadening of the $|m| \leq 1$ modes in Eq. (11) (only), i.e. let $\Gamma_{0,12} \approx \Gamma_{0,1}$ (as has also been confirmed via full Mie scattering calculations). Further dropping the $\delta k_{0,1}$ term in the denominator, yields the peak position relative to the isolated fundamental WGM resonance as:

$$k_{\max} - k_{0,1} \lesssim \frac{\sum_{|m| \leq 1} |D_m|^2 \delta k_{0,1}}{\sum_{2 \leq |m| \leq L} |D_m|^2} \leq \sum_{|m| \leq 1} \frac{\delta k_{0,1}}{2L+1}, \quad (12)$$

where $D_m = \sqrt{(2L)! / [(L+m)!(L-m)!]}$ derive from the Wigner D functions [27]. The first inequality in (12) is satisfied when the NP lies in the plane of the fundamental mode, and follows because coupling is strongest in this case. The latter (weaker) inequality follows by noting the $m = 0$ mode is strongest for a fundamental mode, with mode strength decreasing with increasing $|m|$ (see Figure 2).

Eq. (12) illustrates that to maximise the total apparent shift of the WGM resonance in a typical WGM biosensing experiment, we must maximise the sum of the shifts of the individual $|m| \leq 1$ modes. We perform this optimisation by varying the ratio of the core-shell radii, f , at fixed $k_{0,1}$. Noting that WGMR-NP coupling is weak we

first approximate Eq. (9) further, yielding

$$\delta k_{0,j} = (-1)^j \text{Re} \left[\frac{K + 2ik_1 J}{k_1 - k_2 + iJ} \right]. \quad (13)$$

Eq. (13) is a transcendental equation in $k_{0,12}$, however, as an approximation the translation coefficients (implicit in J and K) are evaluated at the isolated WGM resonance frequency $k_{0,1}$. Resonance shifts then follow by direct evaluation of Eq. (13). An example of such a calculation is shown in Figure 3 for the $j = 1$ (solid lines) and $|m| \leq 1$ quasi-TM modes, as a function of LSP-WGM detuning $\Delta k_{12} = k_{0,1} - k_{0,2}$, with $J = 0$ (i.e. neglecting coupling to off-resonant modes of the WGMR). Shifts of the $j = 2$ (LSP) resonance are also depicted in Figure 3 for reference. Dashed curves in Figure 3 describe shifts determined by exact numerical solution of Eq. (3) and are seen to be shifted to the left relative to the approximate plots, albeit the shift is negligible for the WGM-like modes. Slight narrowing of the transition region is also evident. Larger disparities between the approximate and exact curves for $j = 2$ modes are seen.

Regarding Figure 3 a number of details are worthy of mention. Primarily, as also seen above, clear turning points are exhibited in the $j = 1$ plots, indicating that by judicious choice of NP geometry the shift of the WGM resonance can indeed be maximised. It is further noted that turning points for the $|m| \leq 1$ modes lie in close proximity. Consequently, maximising the sum of shifts is practically equivalent to maximising the individual shifts, since this is achieved for near identical NP geometries (and certainly within current fabrication tolerances). The nature of the apparent WGM shift, however, differs with the sign of the WGM-LSP detuning. Specifically, when the isolated LSP resonance lies at shorter (longer) wavelengths than the WGM resonance, the shift is towards the red (blue) end of the spectrum.

Determination of the optimal NP geometry requires locating the turning points of Eq. (13). Unfortunately, κ_1^E depends on f , complicating the process further. Nevertheless, over the wavelength ranges considered the variation is weak, such that when evaluating κ_1^E , f can be set at a sensible value (here taken such that $\Delta k_{12} = 0$). Performing the stationary point analysis then gives an estimate of the optimal detuning as:

$$\Delta k_{12}^{\text{opt}} = \left[\text{Im}[\tilde{K}] \Delta \Gamma_{12} - \text{Re}[K J^*] + |J|^2 \Gamma_{0,1} \pm \sqrt{|\tilde{K}|^2 (\Delta \Gamma_{12} - 2\text{Im}[J])^2} \right] / \text{Re}[2\tilde{K}] \quad (14)$$

where $\tilde{K} = K + 2ik_1 J$ and $\Delta \Gamma_{12} = \Gamma_{0,1} - \Gamma_{0,2}$.

To proceed, we examine the coupling terms, K and J , further. In Appendix B of [17] it was shown that

$$A_{lm}^{1m} \sim \frac{(l+m)!}{l!} h_{l-1}(z) + \frac{(-1)^m l!}{(l-m)!} h_{l+1}(z) \quad (15)$$

where here $z = n_I k r_{\text{NP}}$ and r_{NP} denotes the NP displacement relative to the WGM. Using the recurrence relations [30] for $h_l(z)$:

$$(2l+1)h_l'(z) = lh_{l-1}(z) - (l+1)h_{l+1}(z) \quad (16)$$

$$\frac{2l+1}{z} h_l(z) = h_{l-1}(z) + h_{l+1}(z) \quad (17)$$

and noting $kr_{\text{NP}} \gg 1$ it follows that:

$$\arg \left[\tilde{\mathcal{A}}_{1,\pm 1}^{l,\pm 1} \mathcal{A}_{l,\pm 1}^{1,\pm 1} \right] = 2 \arctan [y'_l(z)/j'_l(z)] = 2\varphi_l(z) \quad (18)$$

$$\arg \left[\tilde{\mathcal{A}}_{1,0}^{l,0} \mathcal{A}_{l,0}^{1,0} \right] = 2 \arctan [y_l(z)/j_l(z)] = 2\vartheta_l(z) \quad (19)$$

where $y_l(z)$ is the spherical Bessel function of the second kind. Similarly, $\arg[\tilde{\mathcal{B}}_{1m}^{lm} \mathcal{B}_{1m}^{1m}] = 2\vartheta_l(z)$ for $|m| = 1$. The phase functions $\vartheta_l(z)$ and $\varphi_l(z)$ are approximately $\pm\pi/2$ for z smaller than the first zero of $h_l(z)$ and $h'_l(z)$ respectively. Noting the asymptotic expansions for the zeros of $h_l^{(l)}(z)$ [30] and the WGM resonance frequencies [18] and also observing coupling only occurs when the NP is on (or near) the WGM surface (i.e. $r_{\text{NP}} \approx r_{II}$), we find that K is predominantly real when

$$(n_{II} - n_I) L > 2^{-1/3} n_I \alpha_i - n_{II} \beta_1^{(l)}, \quad (20)$$

where α_i denotes the i th negative zero of the Airy function (dictating the radial order of the WGM) and $\beta_1^{(l)}$ denotes the first zero of $h_l^{(l)}(z)$. Inequality (20) is easily satisfied in practice for high Q WGMs. For $|\Delta k_{12}| > |\Delta\Gamma_{12}|/2$, real K implies reactive coupling, i.e. the increase in the half-width of the WGM-like resonance is smaller than the resonance shift (see right inset of Figure 1). If, however, $|\Delta k_{12}| < |\Delta\Gamma_{12}|/2$, i.e. small detunings, coupling becomes resistive even for purely real K , due to the losses of the isolated resonances (as seen from Eq. (13) and its broadening counterpart). In contrast, the J term is dominated by its imaginary part since the $\eta_{l \neq L}^{E,1}$ terms are strongly imaginary away from resonance. Eq. (14) can therefore be approximated as

$$\Delta k_{12}^{\text{opt}} \approx \frac{|\tilde{K}| |\Delta\Gamma_{12} - 2 \text{Im}[J]|}{2 \text{Re}[\tilde{K}]} \approx \left| \frac{\Gamma_{0,2}}{2} + J \right|, \quad (21)$$

where the last step follows for high Q WGMs whereby $|\Delta\Gamma_{12}| \approx \Gamma_{0,2}$. When coupling to $l \neq L$ polar modes is negligible, Eq. (21) states that the optimal WGM resonance shifts are obtained when the LSP of the NP is detuned by half the line-width of the LSP. Spectral overlap of the LSP with other modes within the WGMR, however, produces a shift in this optimal detuning. Induced shifts can be either to greater or smaller detunings, however, noting that the $l \neq L$ modes are excited off-resonance, the effective shift is small. Optimal detunings predicted using Eq. (21) are shown in Figure 3 by the blue arrows. Eq. (21) is thus seen to provide a good rule for optimising core-shell NP geometries and is the main result of this article. Slight numerical differences arise due to the approximations taken.

IV. DISCUSSION

Implicitly, throughout this work it has been assumed that shifts of the $j = 1$, $|m| \leq 1$ resonances are small

relative to their line-widths. If this criterion is not satisfied mode splitting can occur. From Eq. (12) the maximum possible resonance shift is seen to decrease with increasing L (and hence increasing WGMR radius), as illustrated in Figure 2 which plots the ratio $\mathcal{D} = \sum_{|m| \leq 1} |D_m|^2 / \sum_{2 \leq |m| \leq L} |D_m|^2$. Since the line-width of WGM resonances, however, decreases with WGMR radius as $\sim [r_{II} y_L(kr_{II})]^{-2}$ [18], mode splitting is easier to observe in larger WGMRs, albeit this is limited by loss mechanisms, such as NP scattering and absorption [31]. Splitting is hence only observable for a restricted range of NP sizes and is not predicted in this work.

Given that the treatment detailed in this article is largely mathematical, it is important to give a more quantitative estimate of the enhancement of the resonance shifts that may be expected in a typical experiment. Assuming a silica-silver core-shell NP of 55 nm outer radius, we estimate that at the optimal detuning an approximate 90-fold enhancement of the WGM resonance shift can be obtained, as compared to the WGM shift resulting from perturbation by a dielectric sphere of the same dimensions and with a refractive index of 1.5. Use of a gold shell NP reduces the obtainable enhancement to $\sim \times 22$ due to a lower quality LSP resonance. Noting that the maximum near field enhancement (as defined in [32]) arising from a plasmonic NP scales as the square of the polarisability [33], we estimate an enhancement factor of ~ 150 for both gold and silver. A more considered choice of NP materials allows even greater near field enhancements to be achieved [32]. Surface roughness of the NP has also recently been shown to have a significant influence on achievable near field enhancements [12]. Design of the NP to achieve coupling between the WGM and higher order LSP resonances, such as the electric quadrupole resonance, would furthermore allow larger enhancements due to the higher Q of the LSP resonances. Use of more complicated NP geometries allowing greater flexibility and control of the NP spectral properties [19] thus presents an important avenue for plasmon enhanced WGM biosensing, however, binding orientation of asymmetric NPs then also affects the resonance shifts and near field enhancements that can be observed [17].

To summarise, in this article we have considered the use of core-shell NPs as near field nanoantennae or analyte labels for sensing purposes. Improvement of WGM sensors was shown to be possible by tuning the LSP resonance to lie approximately half the LSP (on resonance) line-width from the WGM resonance, whereby an optimal balance of line broadening and shifts is achieved. Sensitivity enhancements were shown to derive from mode hybridisation such that level repulsion played a key role. Criteria under which WGMR-NP coupling is chiefly reactive were also given.

The authors would like to acknowledge financial support from the Max Planck Society.

[1] K. J. Vahala “Optical microcavities” Nature **424**, 839–846 (2003).

[2] W. Ahn, S. V. Boriskina, Y. Hong and B. M. Rein-

- hard “Photonic-plasmonic mode coupling in on-chip integrated optoplasmonic molecules” *ACS Nano*. **6**, 951–960 (2012).
- [3] M. Chamanzar and A. Adibi, “Hybrid nanoplasmonic-photonic resonators for efficient coupling of light to single plasmonic nanoresonators” *Opt. Express* **19** 22292–22304 (2011).
- [4] I. White, J. Gohring, and X. Fan, “SERS-based detection in an optofluidic ring resonator platform” *Opt. Express* **15**, 17433–17442 (2007).
- [5] Y.-F. Xiao, Y.-C. Liu, B.-B. Li, Y.-L. Chen, Y. Li and Q. Gong “Strongly enhanced light-matter interaction in a hybrid photonic-plasmonic resonator” *Phys. Rev. A*, **85**, 031805 (2012)
- [6] H.-C. Ren, F. Vollmer, S. Arnold and A. Libchaber “High-Q microsphere biosensor analysis for adsorption of rodlike bacteria” *Opt. Express* **25**, 17410–17423 (2007).
- [7] M. Noto, D. Keng, I. Teraoka and S. Arnold, “Detection of protein orientation on the silica microsphere surface using transverse electric/transverse magnetic whispering gallery modes” *Biophys. J.* **92**, 4466–4472 (2007).
- [8] F. Vollmer and S. Arnold, “Whispering-gallery-mode biosensing : label-free detection down to single molecules” *Nat. Methods* **5**, 591–596 (2008).
- [9] M. A. Santiago-Cordoba, S. V. Boriskina, F. Vollmer and M. C. Demirel “Nanoparticle-based protein detection by optical shift of a resonant microcavity” *Appl. Phys. Lett.* **99**, 073701 (2011).
- [10] J. Witzens and M. Hochberg, “Optical detection of target molecule induced aggregation of nanoparticles by means of high-Q resonators” *Opt. Express* **19**, 7034–7061 (2011).
- [11] S. Lin and K. B. Crozier “Trapping-assisted sensing of particles and proteins using on-chip optical microcavities” *ACS Nano* **7**, 1725–1730 (2013).
- [12] V. R. Dantham, S. Holler, C. Barbre, D. Keng, V. Kolchenko and S. Arnold “Label-free detection of single protein using a nanoplasmonic-photonic hybrid microcavity” *Nano. Lett.* **13**, 3347–3351 (2013).
- [13] M. A. Santiago-Cordoba, M. Cetinkaya, S. V. Boriskina, F. Vollmer and M. C. Demirel, “Ultrasensitive detection of a protein by optical trapping in a photonic-plasmonic microcavity” *J. Biophot.* **5**, 629–638 (2012).
- [14] C. F. Bohren and D. R. Huffman *Absorption and scattering of light by small particles* (John Wiley & Sons, Inc, Weinheim 1998).
- [15] R. K. Chang, (ed.) *Optical Processes in Microcavities* (World Scientific, Singapore, 1996)
- [16] E. S. C. Ching, P. T. Leung, A. Maassen van den Brink, W. M. Suen, S. S. Tong and K. Young, “Quasinormal-mode expansion for waves in open systems” *Rev. Mod. Phys.* **70**, 1545–1554 (1998).
- [17] M. R. Foreman and F. Vollmer “Theory of resonance shifts of whispering gallery mode sensors by arbitrary plasmonic nanoparticles” *New. J. Phys.* **15**, 083006 (2013).
- [18] C. C. Lam, P. T. Leung and K. Young “Explicit asymptotic formulas for the positions, widths, and strengths of resonances in Mie scattering” *J. Opt. Soc. Am. B* **9**, 1585–1592 (1992).
- [19] V. Giannini, A. I. Fernández-Domínguez, S. C. Heck and S. A. Maier, “Plasmonic nanoantennas: fundamentals and their use in controlling the radiative properties of nanoemitters” *Chem. Rev.* **111**, 3888–3912 (2011).
- [20] D. W. Mackowski, R. A. Altenkirch and M. P. Menguc “Internal absorption cross sections in a stratified sphere” *Appl. Opt.* **29**, 1551–1559 (1990).
- [21] P. C. Waterman, “New formulation of acoustic scattering” *J. Acoust. Soc. Am.* **45**, 1417–1429 (1969).
- [22] A. Moroz, “Depolarization of spheroidal particles” *J. Opt. Soc. Am. B* **26**, 517–527 (2009).
- [23] N. Halas, “The Optical Properties of Nanoshells,” *Opt. Photon. News* **13**, 26–30 (2002).
- [24] U. Kreibig, “Electronic properties of small silver particles: the optical constants and their temperature dependence” *J. Phys. F: Metal Phys.* **4**, 999–1014 (1974).
- [25] X. Miao, I. Brener, and T. S. Luk “Nanocomposite plasmonic fluorescence emitters with core/shell configurations” *J. Opt. Soc. Am. B* **27**, 1561–1570 (2010).
- [26] S. Arnold, M. Khoshshima, I. Teraoka, S. Holler, and F. Vollmer, “Shift of whispering-gallery modes in microspheres by protein adsorption” *Opt. Lett.* **28**, 272–274 (2003).
- [27] L. Deych and J. Rubin “Rayleigh scattering of whispering gallery modes of microspheres due to a single dipole scatterer” *Phys. Rev. A* **80**, 061805 (2009).
- [28] A. Serpengüzel, S. Arnold, G. Griffel and J. A. “Lock Enhanced coupling to microsphere resonances with optical fibers” *J. Opt. Soc. Am. A* **14**, 790–795 (1997).
- [29] J. D. Jackson, *Classical Electrodynamics* (John Wiley & Sons, New York, 1998).
- [30] M. Abramowitz and I. Stegun, *Handbook of Mathematical Functions* (Dover, 1970).
- [31] Ş. K. Özdemir, J. Zhu, L. He and L. Yang, “Estimation of Purcell factor from mode-splitting spectra in an optical microcavity” *Phys. Rev. A* **83**, 033817 (2011).
- [32] K. Tanabe “Field Enhancement around Metal Nanoparticles and Nanoshells: A Systematic Investigation” *J. Phys. Chem. C* **112**, 15721–15728 (2008).
- [33] M. R. Foreman, Y. Sivan, S. A. Maier and P. Török “Independence of plasmonic near-field enhancements to illumination beam profile” *Phys. Rev. B* **86**, 155441 (2012).